

# **AlGaN Channel Transistors for Power Management and Distribution.**

Final Report  
Phase I SBIR Contract N00014-96-C-0251  
December 30, 1996

Submitted to:

Dr. Colin Wood, Code 312  
Program Officer  
Office of Naval Research  
800 North Quincy Street  
Arlington, Virginia 22217-5660

Submitted by:

Dr. James M. Van Hove  
SVT Associates  
7620 Executive Drive  
Eden Prairie, MN 55344  
(612) 934-2100 ext. 225  
(612) 934-2737 Fax  
jvanhove@svta.com

## **DISTRIBUTION STATEMENT A**

Approved for public release;  
Distribution Unlimited

19970106 059

DEFENSE QUALITY INSPECTED 1

# REPORT DOCUMENTATION PAGE

Form Approved  
OMB No. 0704-0188

Public reporting burden for this collection of information is estimated to average 1 hour per response, including the time for reviewing instructions, searching existing data sources, gathering and maintaining the data needed, and completing and reviewing the collection of information. Send comments regarding this burden estimate or any other aspect of this collection of information, including suggestions for reducing this burden, to Washington Headquarters Services, Directorate for Information Operations and Reports, 1215 Jefferson Davis Highway, Suite 1204, Arlington, VA 22202-4302, and to the Office of Management and Budget, Paperwork Reduction Project (0704-0188), Washington, DC 20503.

1. AGENCY USE ONLY (Leave Blank)		2. REPORT DATE December 30, 1996		3. REPORT TYPE AND DATES COVERED Final Report. 4/30/96 to 10/30/96	
4. TITLE AND SUBTITLE  AlGa <sub>N</sub> Channel Transistors for Power Management and Distribution				5. FUNDING NUMBERS  N00014-96-C-0251	
6. AUTHOR(S)  Dr. James M. Van Hove				7. PERFORMING ORGANIZATION NAME(S) AND ADDRESS(ES)  SVT Associates, Inc. 7620 Executive Drive Eden Prairie, MN 55344	
8. SPONSORING/MONITORING AGENCY NAME(S) AND ADDRESS(ES)  Office of Naval Research Ballston Tower One 800 North Quincy Street Arlington, VA 22217-5660				9. PERFORMING ORGANIZATION REPORT NUMBER	
10. SUPPLEMENTARY NOTES				11. SPONSORING/MONITORING AGENCY REPORT NUMBER	
12a. DISTRIBUTION/AVAILABILITY STATEMENT  Approved for Public Release, Distribution is Unlimited				12b. DISTRIBUTION CODE	
13. ABSTRACT (Maximum 200 words)  Contained within is the Final report of a Phase I SBIR program to develop AlGa <sub>N</sub> channel junction field effect transistors (JFET). The report summarizes our work to design, deposit, and fabricate JFETS using molecular beam epitaxy grown AlGa <sub>N</sub> . Nitride growth is described using a RF atomic nitrogen plasma source. Processing steps needed to fabricate the device such as ohmic source-drain contacts, reactive ion etching, gate formation, and air bride fabrication are documented. SEM photographs of fabricated power FETS are shown. Recommendations are made to continue the effort in a Phase II Program.					
14. SUBJECT TERMS  High temperature electronics, AlGa <sub>N</sub> , JFET RF Plasma Nitrogen, Power management and distribution				15. NUMBER OF PAGES	
17. SECURITY CLASSIFICATION OF REPORT  Unclassified				18. SECURITY CLASSIFICATION OF THIS PAGE  Unclassified	
19. SECURITY CLASSIFICATION OF ABSTRACT  Unclassified				20. LIMITATION OF ABSTRACT  unlimited	

## Table Of Contents

1.0 Phase I Technical Objectives/Summary .....	3
2.0 Phase I Research Description, Technical Data and Results. ....	4
2.1 Modeling and Device Designs. ....	4
2.2 MBE Nitride growth.....	9
2.2.1 RF Source.....	9
2.2.2 Enhanced 2-deg Mobility.....	11
2.2.3 P type GaN.....	12
2.2.5 In-situ Characterization -in-situ Cathodoluminescence .....	13
2.3 FET Processing .....	15
2.3.1 High Temperature Ohmic Contacts.....	18
2.4 JFET Test and Measurement .....	23
3.0 Conclusions and Recommendations.....	26
4.0 Appendix.....	27

## **1.0 Phase I Technical Objectives/Summary**

The final goal of this SBIR program is to demonstrate a commercially viable high temperature power switching FET for PMDA applications. During the Phase I (6 month) effort, excellent progress was achieved using AlGa<sub>N</sub> deposited by Molecular Beam epitaxy onto sapphire substrates. Operational JFETs were not achieved during the Phase I effort, but the cause of the device failures have been identified. Working JFETs are expected by the Phase II proposal submission. Below is listed the specific objectives of the program from the Phase I proposal and a brief summary of the work conducted.

**1. Device Modeling.** An intrinsic and a doped channel HEMT type structure using an AlGa<sub>N</sub> barrier on a Ga<sub>N</sub> channel were designed with a gate pinchoff voltage near 5 V. This design was then deposited and fabricated into JFETs.

**2. Material Deposition.** The AlGa<sub>N</sub> JFET structures were deposited in a molecular beam epitaxy system using a RF plasma source for active nitrogen. Improvements to the P type doping control and film morphology were done. Low temperature Hall on the HEMT structure (measurement done by NASA Lewis) indicated enhanced 2-deg. mobility. In-situ cathodoluminescence was developed in part to characterize the deposited films. This work was presented at the 1996 International MBE conference. A copy of the paper is included in the Appendix.

**3. Mask layout.** A six level JFET mask was designed and procured from a mask vendor. A total of 90 distinct JFET structures are contained within each repeated die on the mask plate. Process control monitors were added for ohmic contacts, breakdown, isolation, etc.

**4. Device Fabrication.** This task represents the major effort of the Phase I program. The processing steps of mesa isolation, ohmic contact formation, gate recessing, and air bridge formation were developed specifically for AlGa<sub>N</sub> JFETs. AlGa<sub>N</sub> JFETs were fabricated and device failure modes identified.

**5. Material and Device Test.** The JFETs were electrically tested and did not yield working devices. The problem appears to be the P type RIE gate recess causing damage to the Ni/Au gate region. Processing is being modified to achieve working devices. Ohmic contacts were tested at elevated temperature to determine contact reliability. HEMT mobility structures were characterized by Hall as a function of temperature.

**6. Recommendation.** The Phase I program was extremely successful. Enhanced mobility was observed in AlGa<sub>N</sub> HEMT structures. A JFET mask set was designed and used to develop the processing steps needed for JFET fabrication. Several two inch wafers of AlGa<sub>N</sub> JFET structures were fabricated and tested. Based on the success of the six month program, we are now in discussion with two investment groups for the matching Phase II funding required by BMDO. We strongly recommend continued funding of this program.



## 2.0 Phase I Research Description, Technical Data and Results.

This section outlines the research conducted under the Phase I program. Technical details related to the objectives summarized in the first section are included. The program was conducted at SVT Associates in Eden Prairie, MN. Processing of the JFET was done at the University of MN by SVT Associates.

### 2.1 Modeling and Device Designs.

#### A) JFET epitaxial structures

The first epitaxial designs used for deposition were both an intrinsic and a doped channel HEMT-type structure employing an AlGa<sub>N</sub> barrier on a Ga<sub>N</sub> channel. Depletion calculations were performed to estimate the p-type Ga<sub>N</sub> and n-type AlGa<sub>N</sub> to yield charge control of a channel electron sheet density from  $1 \cdot 10^{13}$  to  $4 \cdot 10^{13} \text{ cm}^{-2}$ . The first epitaxial designs are intended to be depletion mode JFETs with a gate pinchoff voltage near 5 V. The epitaxial structures are listed in Table 1 and 2.

	Doping Level	Material	Thickness (Å)
Layer 5:	1-3e18	<i>p</i> -Ga <sub>N</sub>	1000
Layer 4:	1-2e18	<i>n</i> -AlGa <sub>N</sub>	250
Layer 3:	1-2e18	<i>n</i> -Ga <sub>N</sub>	100
Layer 2:	<i>intrinsic or SI</i>	<i>i</i> -Ga <sub>N</sub> buffer	1.0 μm
Layer 1:	SI	AlN buffer	
Substrate		Sapphire	

Table 1: Doped channel AlGa<sub>N</sub>/Ga<sub>N</sub> JFET epitaxial structure.

	Doping Level	Material	Thickness (Å)
Layer 4:	1-3e18	<i>p</i> -Ga <sub>N</sub>	1000
Layer 3:	1-2e18	<i>n</i> -AlGa <sub>N</sub>	300
Layer 2:	<i>intrinsic</i>	<i>i</i> -Ga <sub>N</sub> buffer	1.0 μm
Layer 1:	SI	AlN buffer	
Substrate		Sapphire	

Table 2: Intrinsic channel AlGa<sub>N</sub>/Ga<sub>N</sub> JFET epitaxial structure.

The two JFET epitaxial structures investigated include an intrinsic channel structure and a doped channel structure. The impurity ionization scattering in Ga<sub>N</sub> is expected to possess a reduced influence the 2-DEG mobility in comparison to other materials systems such as GaAs or InP. Therefore, it is worthwhile to investigate the performance trade-offs of doping the channel to obtain higher 2-DEG sheet densities and greater power density.

## B) Mask set

A six layer JFET mask was designed and procured from a mask vendor. The six plates were designed for 1) patterning of alignment marks, 2) mesa isolation, 3) source and drain (S/D) contact deposition, 4) p-type gate deposition, and 5/6) air bridge and bond pad gold plating. A total of 90 distinct JFET structures are contained within each repeated die on the mask plates. The individual die size is 7.2 by 7.8 mm. In addition, each die includes transmission line measurement (TLM) structures to determine both n- and p-type contact resistances for the S/D and gate, respectively. There are also five p-n diode test structures, and metal step coverage process monitoring structures. A composite layout of the die pattern is given in Figure 1.

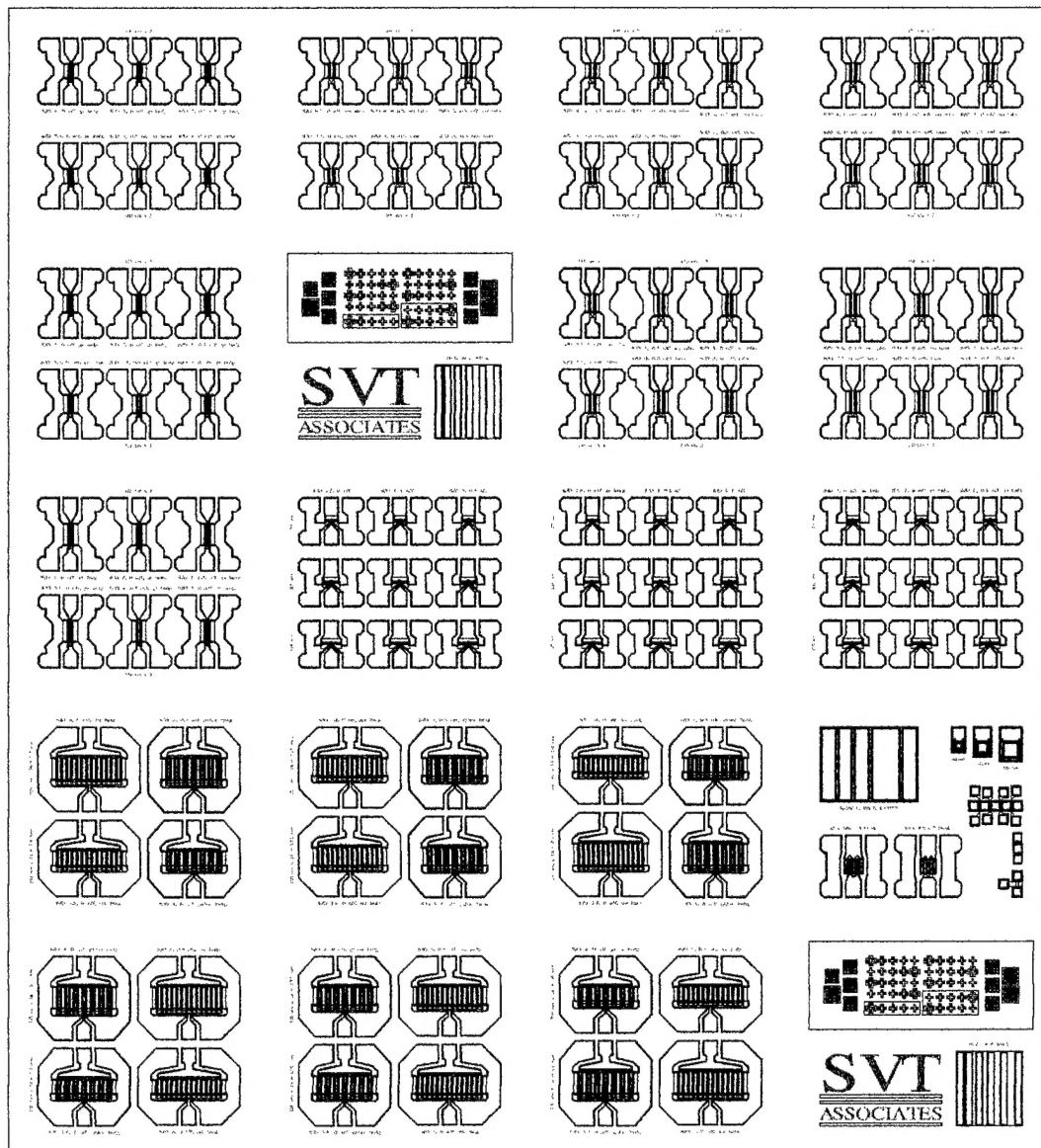


Figure 1. Composite drawing of Mask Set designed for the Phase I program.

Of the 90 JFET designs, a wide variety of geometries exist for device testing. The transistors range from simple dual-gate finger structures (Figure 2) for fundamental testing to 14-gate finger structures for high power testing (Figure 3). All devices were based on 1  $\mu\text{m}$  gate lengths, but the gate widths include 100, 125 and 150  $\mu\text{m}$  to evaluate the frequency response effects of distributed gate resistance and phase modulation along the gate structure. Therefore, the total gate width of the JFETs range from 0.2 mm for a small signal or low noise type transistor to 2.1 mm for a power transistor to switch several watts of electrical power. S/D spacing are varied at 3.5, 4.0 and 5.0  $\mu\text{m}$  to eventually investigate a potential increase in the gate/source breakdown voltage as the gates are patterned closer to the source contact. Devices with S/D spacing of 4 and 5  $\mu\text{m}$  were designed with gates offset toward the source by 0.5  $\mu\text{m}$  in addition to those with no offset. Finally, the JFETs were equally divided between devices which have the gate metallization deposited up the mesa edge (Figure 4) and devices which have the gate isolated from the edge with an air bridge to the contact pad (Figure 5). The purpose of airbridged gates is to study the gate bias leakage current resulting from gate contact on the mesa sidewall.

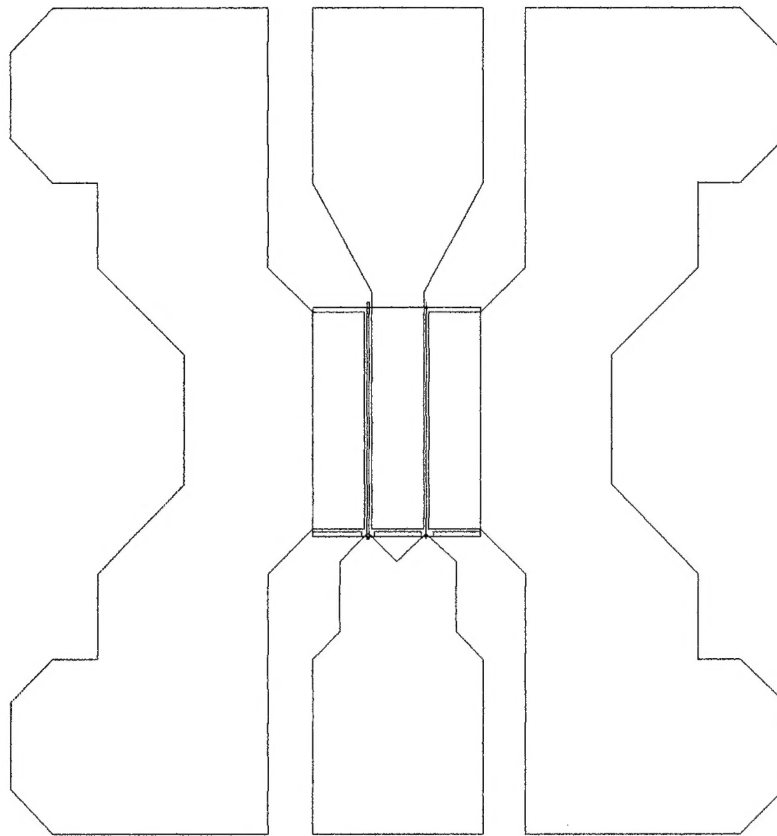


Figure 2. Dual gate FET layout.

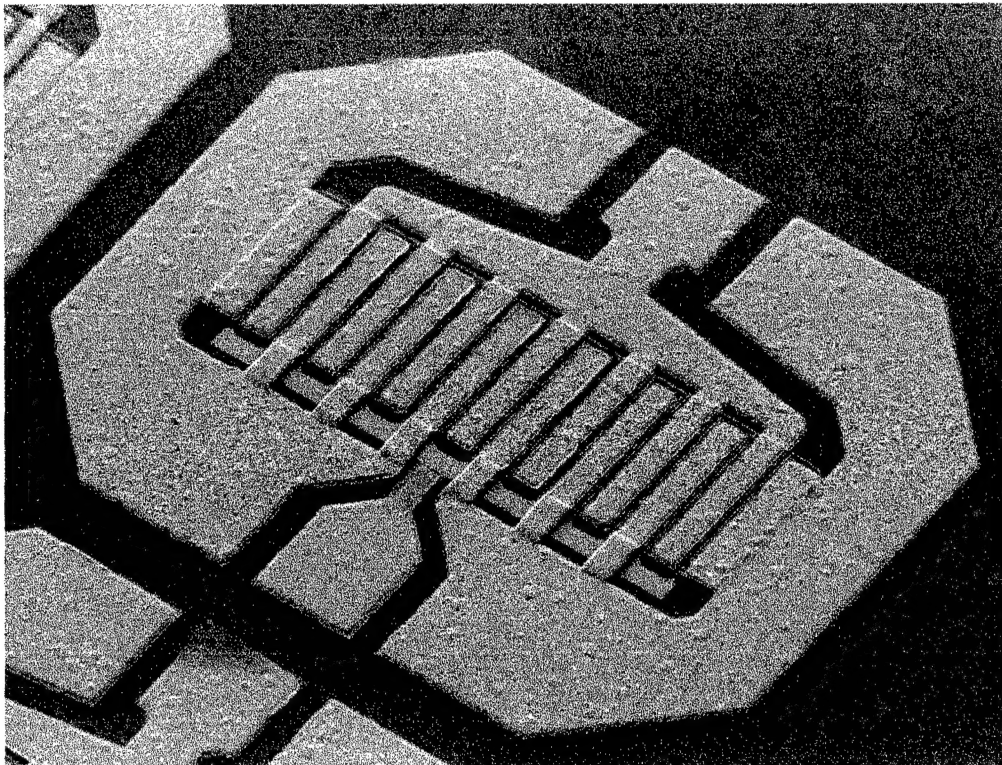
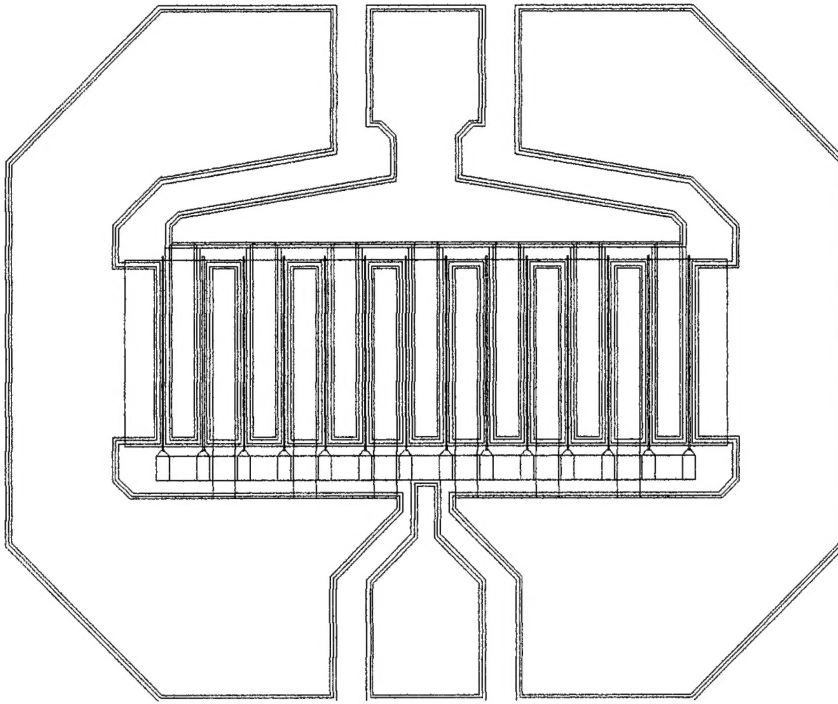


Figure 3. Power JFET composite mask drawing and SEM of fabricated JFET with air bridges.

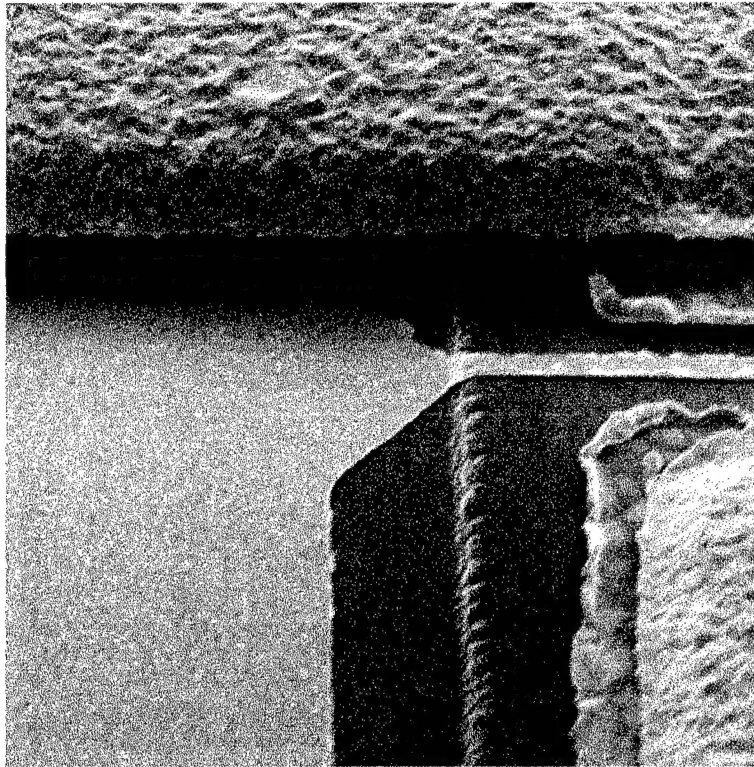


Figure 4. SEM of fabricated AlGaIn JFET showing gate metal running up MESA edge.

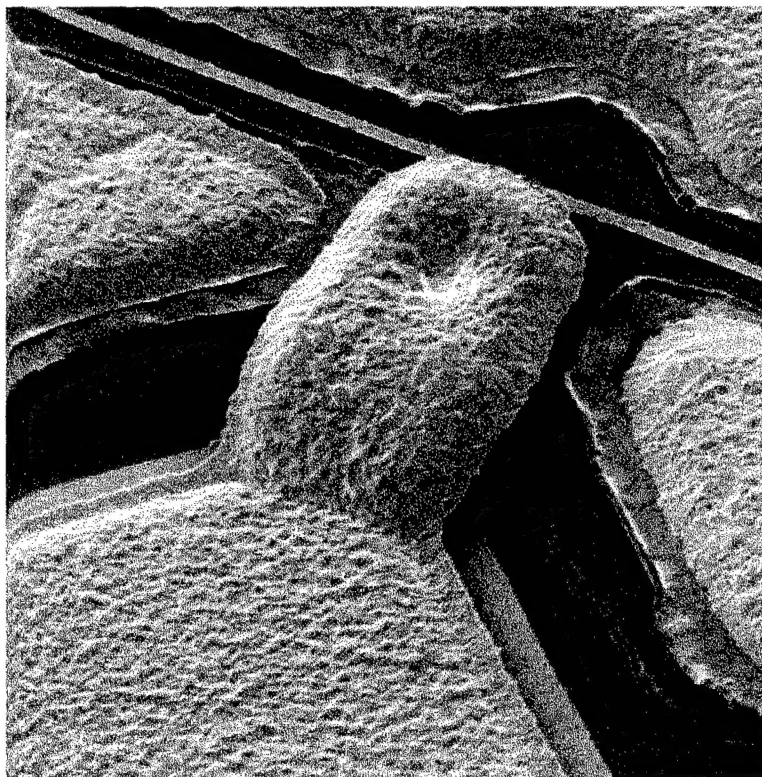


Figure 5. SEM of Airbridge gate contact to AlGaIn JFET.



## 2.2 MBE Nitride growth

The MBE system used for the Phase I effort at SVT Associates is shown in Figure 6. This is a Perkin Elmer 425B system originally designed for the growth of GaAlAs compounds. Elemental Ga and Al heated in MBE effusions cells were used for the nitride deposition. The substrate heater was modified to allow higher growth temperatures. The system has  $\text{LN}_2$  cryopanel panels to reduce background levels and is pumped during growth with a cryopump. Si doping was done with a e-beam heated Si source capable of producing doping levels from  $10^{20}$  to  $10^{17} \text{ cm}^{-3}$ . Mg P type doping was done with a Mg source.,

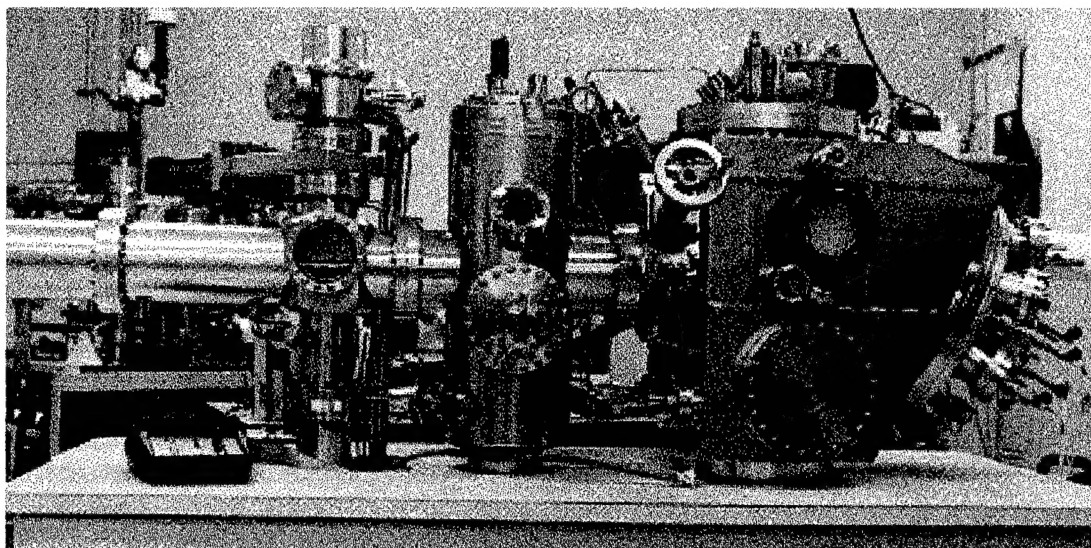


Figure 6. Modified Perkin Elmer 425B MBE modified for Nitride depositions at SVT Associates.

### 2.2.1 RF Source

The most important component of this MBE system is the RF plasma source that creates activated Nitrogen. Figure 7 shows a line drawing of the source which has been sold to many different research groups. The basic concept is to create a plasma with the use of a RF field. RF energy (about 300 W) is fed into the gun through a water cooled copper coil. A PBN tube with a changeable nozzle is centered between the RF coils. Gas is introduced to the tube with a leak valve or a mass flow controller. Under certain power levels and flow rates a plasma is created within the tube. An optical port located at the rear of the gun allows us to monitor the plasma with an optical spectrometer to determine what excited species are present. By adjusting the operating conditions, we can change the amount of excited molecular, atomic or ionic species produced. We have achieved growth rates as high as  $1 \mu\text{m/hr}$  using this source. Figure 8 shows a photograph of an early version of this source with a quartz reaction tube. The photograph clearly shows the a nitrogen plasma and the copper RF coils. The optical port located at the rear of the gun allows the emission levels of the plasma to be monitored.

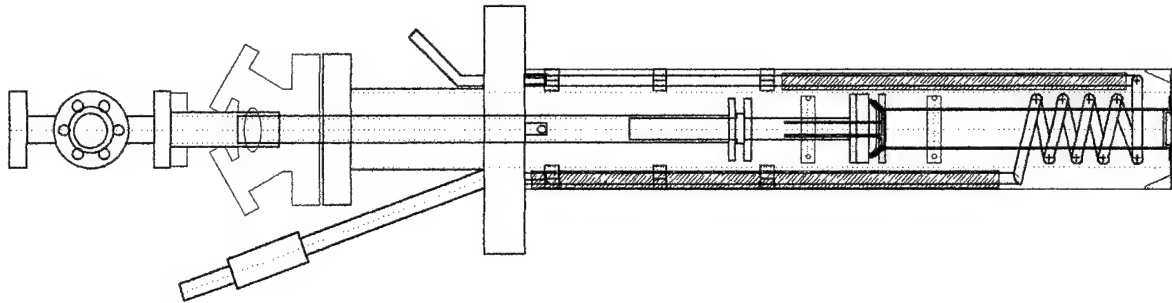


Figure 7. Line drawing of the SVT Associates RF plasma source used for creating reactive atomic nitrogen plasma.



Figure 8. Photograph showing RF source without RF shield and glow from nitrogen. A quartz tube is shown for the photograph. A reaction chamber made of PBN is used for nitride growth.

Basal Plane (0001) sapphire was used as a substrate during this contract. The sapphire was initially degreased in ACE and ISO and blown dry with Nitrogen. The samples were then etched in 3:1 solution of  $\text{H}_2\text{SO}_4:\text{H}_3\text{PO}_4$  heated to  $50^\circ\text{C}$  for 15 to 45 minutes. The sapphire was then rinsed in ISO and blown dry. Since the sapphire is transparent to IR and visible, heating the sample uniformly is quite difficult. We have found that by evaporating a metallic layer of either Mo or Ti on the back of the substrate and using a non-bonded block (wafer sees the heater directly), the sapphire can be heated to temperatures of  $1200^\circ\text{C}$ . After loading the samples into the MBE system, they were ramped up to  $1050^\circ\text{C}$  to clean the sapphire for 15 minutes. The substrate temperature is then reduced and a low temperature ( $100^\circ\text{A}$ ) AlN buffer layer was grown at  $500^\circ\text{C}$ . The substrate was then heated to around  $800^\circ\text{C}$  for the GaN growth. Typical growth temperatures used for GaN was  $800$  to  $850^\circ\text{C}$ .  $P_g$  was  $3 \times 10^{-5}$  Torr and the RF power was  $350$  W. Growth rates for the GaN and AlGaIn layers were around  $0.5 \mu\text{m/hr}$ . After growth, the Mo backside metal layer was chemically removed.

### 2.2.2 Enhanced 2-deg Mobility

An initial task was to deposit and characterize a MODFET or HEMT structure without the P GaN cap. A structure similar to the intrinsic channel JFET shown in Table 2 without the top P layer was grown. Hall bars were fabricated and the sample was mounted on a ceramic chip carrier with gold wirebonds. NASA Lewis measured the mobility and sheet carrier concentration as a function of temperature. Figure 8 shows a room temperature mobility of  $550 \text{ cm}^2\text{V}^{-1}\text{s}^{-1}$  increasing to  $1200 \text{ cm}^2\text{V}^{-1}\text{s}^{-1}$  at  $4 \text{ K}$ . The sheet charge density decreased from  $1.5 \times 10^{13} \text{ cm}^{-2}$  to around  $1 \times 10^{13} \text{ cm}^{-2}$  from room to  $4 \text{ K}$ . We attribute the enhanced mobility to the formation of a 2-deg at the AlGaIn/GaN interface. Significant improvement in this value should be expected as AlGaIn growth conditions and buffer layer smoothness is improved.

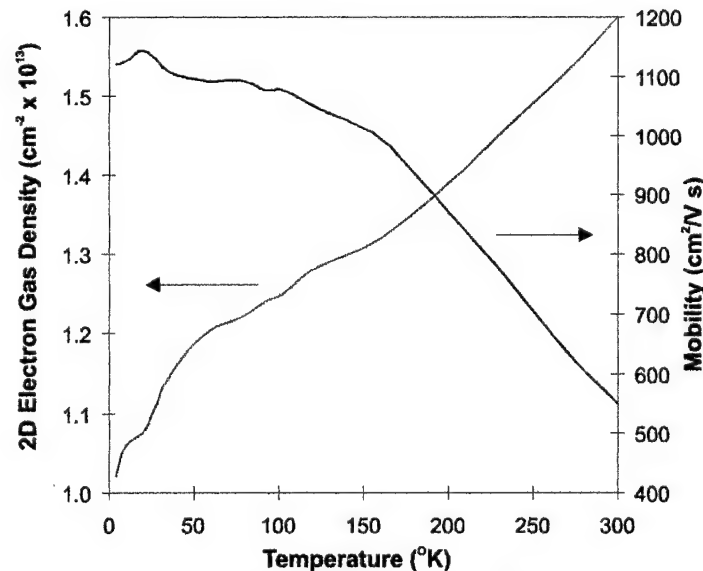


Figure 8. Mobility and sheet charge density for AlGaIn HEMT structure. Measurement done by NASA Lewis.



### 2.2.3 P type GaN.

Another area which needed attention during the Phase I program was the deposition of heavy doped P type GaN. Mg is used for the P type doping and is supplied from an effusion cell operating between 300 to 500°C. Due to the high vapor pressure of Mg and the 800°C growth temperature, a very small amount of the incident Mg is incorporated into the GaN. Our initial growth process was to increase the Nitrogen flux so the III-V ratio was around 1:2. This resulted in increased Mg incorporation, but a rough morphology as shown in Figure 9 resulted. Clearly this morphology was inadequate for 1  $\mu\text{m}$  gate lithography. During the Phase I program, we found that a III-V flux ratio of 1:1 resulted in improved morphology but reduced Mg incorporation. A side view SEM of the smooth P type film is shown in Figure 10. The substrate temperature was then varied slightly. We found that a 15 degree change in substrate temperature results in a 2 times change in doping density for a given Mg flux. This strong dependence upon substrate temperature implies for future production JFET epitaxy growth, both the substrate temperature uniformity and the temperature reproducibility will have to be improved. We are now capable of doping P type GaN from low  $10^{17} \text{ cm}^{-3}$  to  $5 \times 10^{18} \text{ cm}^{-3}$ .

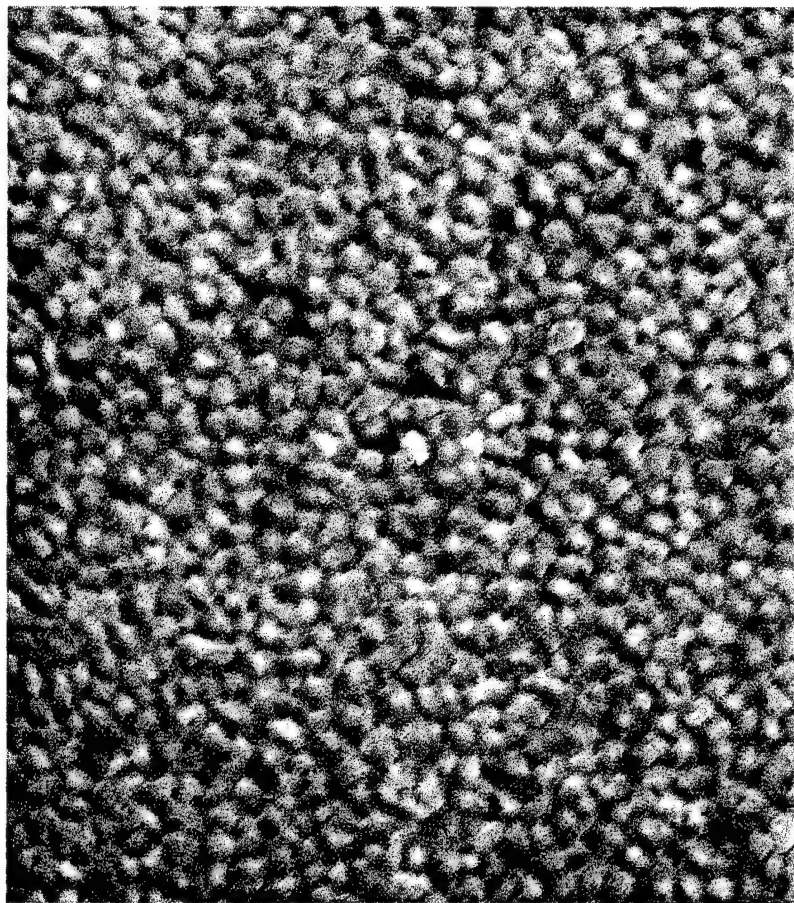


Figure 9. Rough surface morphology of heavy P type GaN grown under high V:III flux ratios. View is 4  $\mu\text{m}$  by 6  $\mu\text{m}$ .



Figure 10. Side view SEM of 1  $\mu\text{m}$  of P type GaN showing much smoother surface morphology grown under 1:1 V:III flux ratios.

### 2.2.5 In-situ Characterization -in-situ Cathodoluminescence

Several standard in-situ characterization techniques were used during this program such as RHEED and Auger. A third method which we have found extremely useful for nitride growth is in-situ Cathodoluminescence (CL). In CL, an electron beam is used to excite the sample which emits light in a similar fashion as Photoluminescence. We equipped our MBE system with a CL system in the Analysis chamber that allows us to measure the intensity vs wavelength characteristics of our material without removing the sample from the system. A version we have fabricated for the growth chamber is shown in Figure 11. By changing the incident e-beam energy, profiling of the CL vs depth into the film is obtained. Changes in the growth conditions can be made, CL measured, and new conditions tried to optimize the material's optical quality including removal of the yellow emission band commonly observed in GaN. Determination of the Al content is done by measuring in-situ the bandedge emission from the AlGaIn film. Emission of MQW structures can be measured in-situ to optimize the wavelength and intensity. Figure 12 shows various CL scans taken during deposition of a in-plane laser structure consisting of 5 and 11% AlGaIn clad layers and a GaN active region. This work, developed in part under this program was presented at the 1996 International MBE conference. A publication based on our work with in-situ CL is included in the Appendix and includes CL's ability to measure substrate temperature, film composition, optical quality, and doping incorporation. CL proved extremely useful for determining Mg doping levels without removing the sample from the chamber. These results are described in the paper in the Appendix.

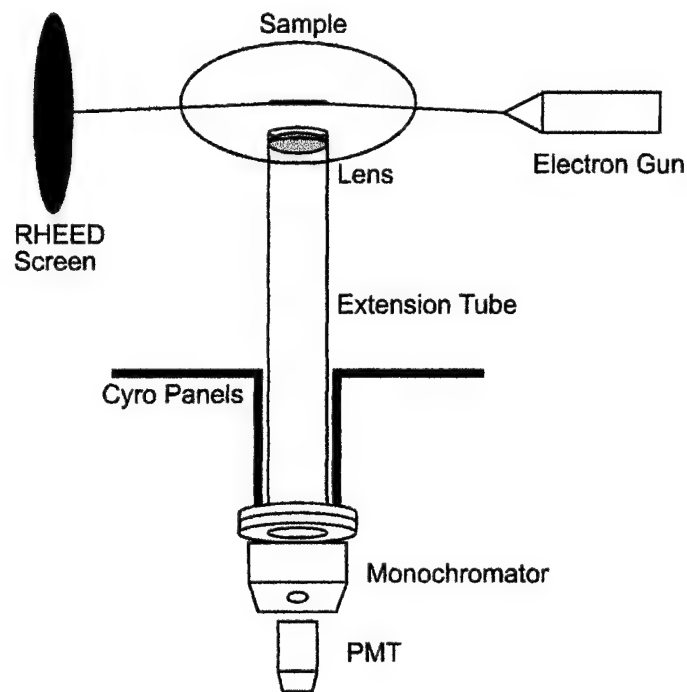


Figure 11. In-situ CL used to determine optical quality, Al composition, and doping of Nitride films

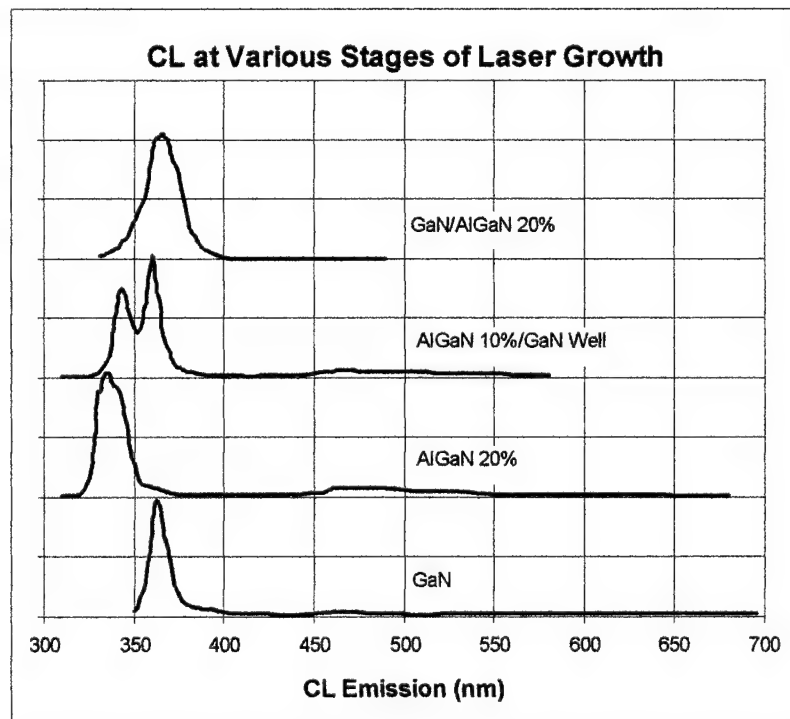


Figure 12. CL of in-plane laser showing the 20% Clad layers, and the MQW emission area.

## 2.3 FET Processing

A significant amount of process development was performed under the Phase I program to modify existing photolithography processes to the JFET development effort. All wafers processed were full 2" diameter as seen in Figure 13 and not cleaved sections. A schematic outline of the JFET process is given in Figure 14.

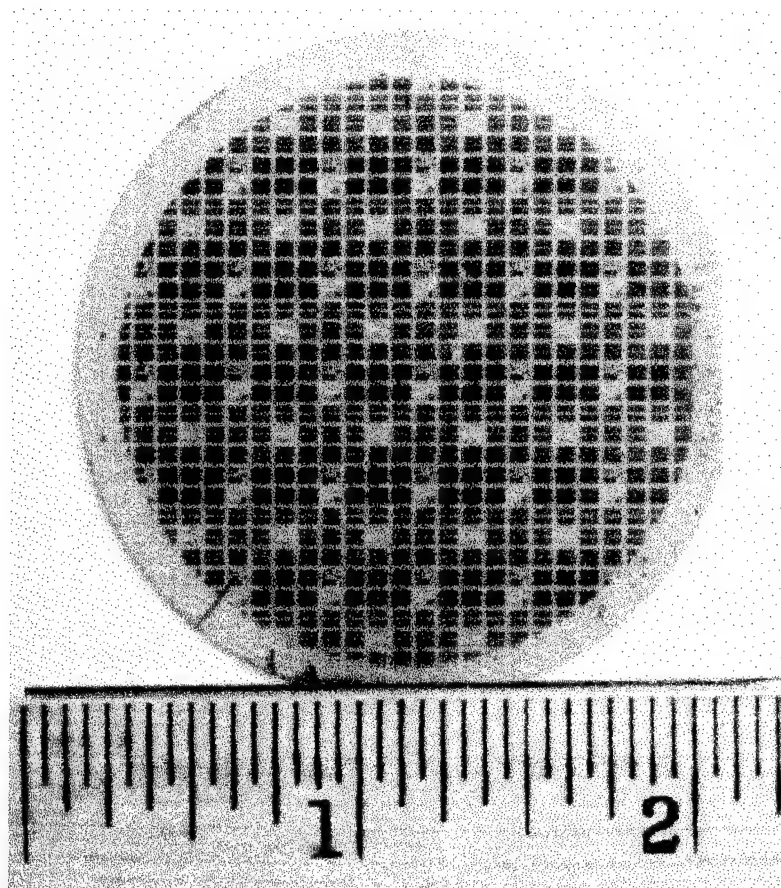


Figure 13. Photograph of processed AlGaIn JFET on a two inch sapphire substrate.

The JFET process sequence began with the deposition of a pattern of master **alignment marks** on the wafer to maintain layer-to-layer registration during the photolithography sequence. The master alignment marks were patterned by liftoff of Ti/Au (500/200 Å) using an i-line resist optimized to reduce standing UV exposure waves and maintain critical dimension uniformity. Close attention to detail of the master alignment mark deposition allowed for more accurate registration of the S/D and gate deposition layers. Registration control is important in achieving yield for the transistor structures based on 3.5 mm S/D spacing and structures based on gates closely offset toward the source.

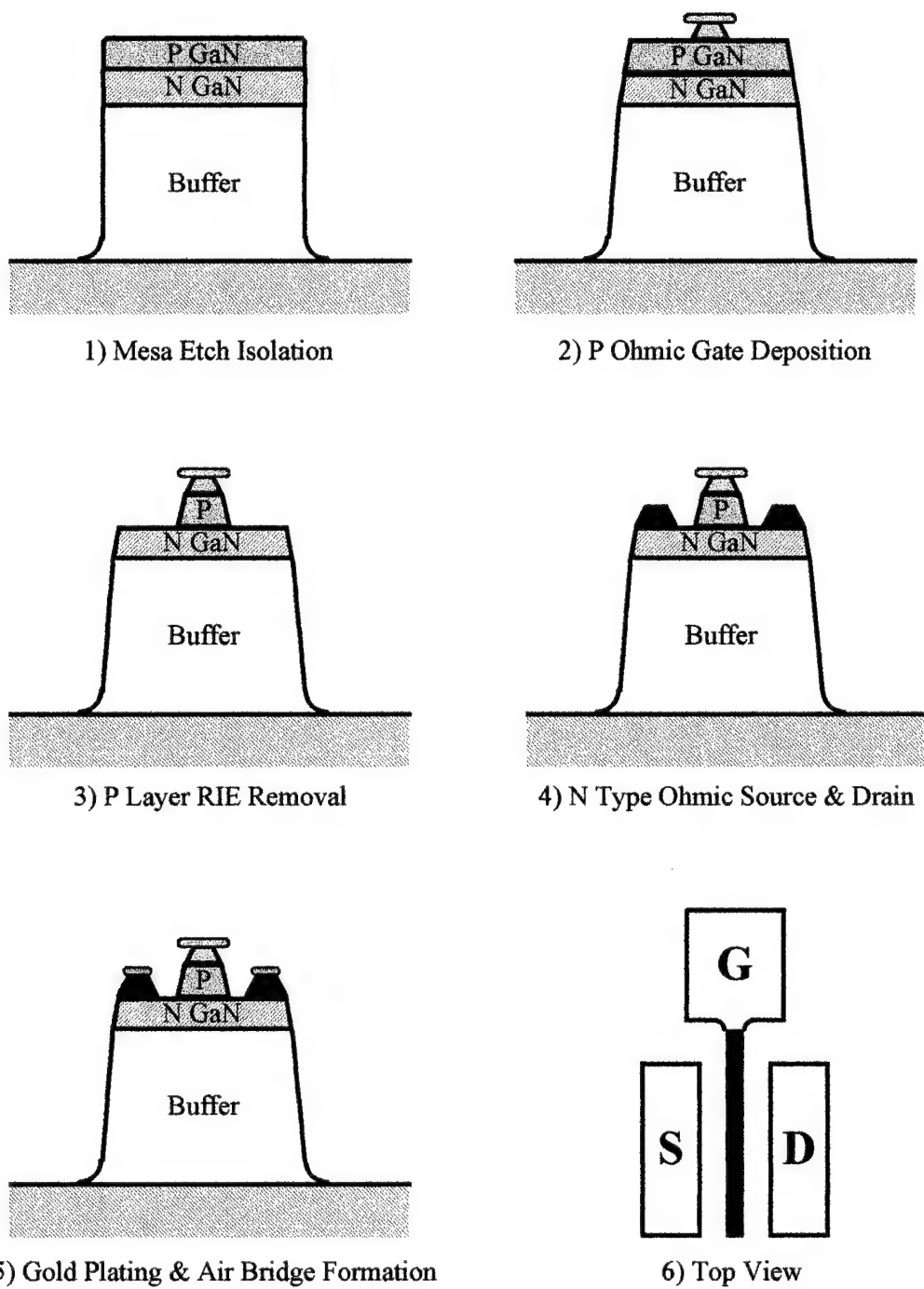


Figure 14. Process flow diagram for AlGaIn JFET.

The next step in the fabrication process involved etching of the **mesa isolation** structures for the JFETs. The mesa islands were etched using a parallel plate reactive ion etch (RIE) in  $\text{SiCl}_4$  plasma. A 6 sccm  $\text{SiCl}_4$  plasma gas flow optimized at 60-90 W RF power and 6-10 mT chamber pressure is employed to achieve etch rates over the range of 100 to  $>600 \text{ \AA}/\text{min}$ . The photoresist mask pattern proved to be most stable in the pure  $\text{SiCl}_4$  (without Ar added by others) plasma at 6 sccm, 10 mT, and 80 W with a GaN etch rate of approximately  $250 \text{ \AA}/\text{min}$ .

An optimized fine line process using i-line resist was employed to pattern the 1.0 mm **gates** by liftoff technique. Ni/Au gates were deposited in the p+-GaN. The gate metal acted as a masking layer in the next step which was to **recess** the remaining p+-GaN layer to expose the n-AlGaN layer for S/D contact lithography. A 10 sccm gas flow of  $\text{SiCl}_4$  at 50 mT and 60 W was in the parallel plate RIE process to perform the recess.

After the gate structures were completed, the **S/D contacts** were deposited. This again involved patterning the wafer using an i-line resist and liftoff of Ti/Mo/Au. The deposition of the Mo layer still need to be improved. The e-beam evaporator does not have a cooling stage for the wafers. The high temperature Mo deposition causes the resist to reflow resulting in rough edges as seen in Figure 3-5 in this report. This can be corrected by installing a cooling stage. The contacts were then annealed in a rapid thermal anneal system at  $400^\circ \text{C}$  for 30 seconds in a nitrogen ambient. Higher temperatures were not employed to prevent peeling of the Ni/Au metal at the gate.

After the gates were successfully laid down, the critical process of fabricating **airbridges** then followed. Another mask layer of i-line resist was patterned with an additional hard bake step of  $130^\circ \text{C}$  for 90 seconds to induce reflow. A seed layer of Ti/Au was evaporated on top of the patterned resist. The final processing layer of resist was patterned on top of the seed layer for the airbridge structures, and the wafer was then ready for plating. The plating process was based on a commercial solution. The wafer was plated using a DC current with a resulting plating rate of about  $120 \text{ \AA}/\text{min}$ . Airbridge thicknesses ranged from 1-3 mm. Low DC currents allowed for the plating of fine lines and minimum resist damage. The seed layer of Ti/Au was removed using a Au de-plate solution followed by a 10:1 buffered oxide etch (BOE) acid dip. In order to remove all resist trapped under the airbridges, the wafer was stripped using a commercial heated resist strip and ultrasonic treatment. Microimages of the airbridges for power FET (2.1 mm gate width) are shown in Figure 15.



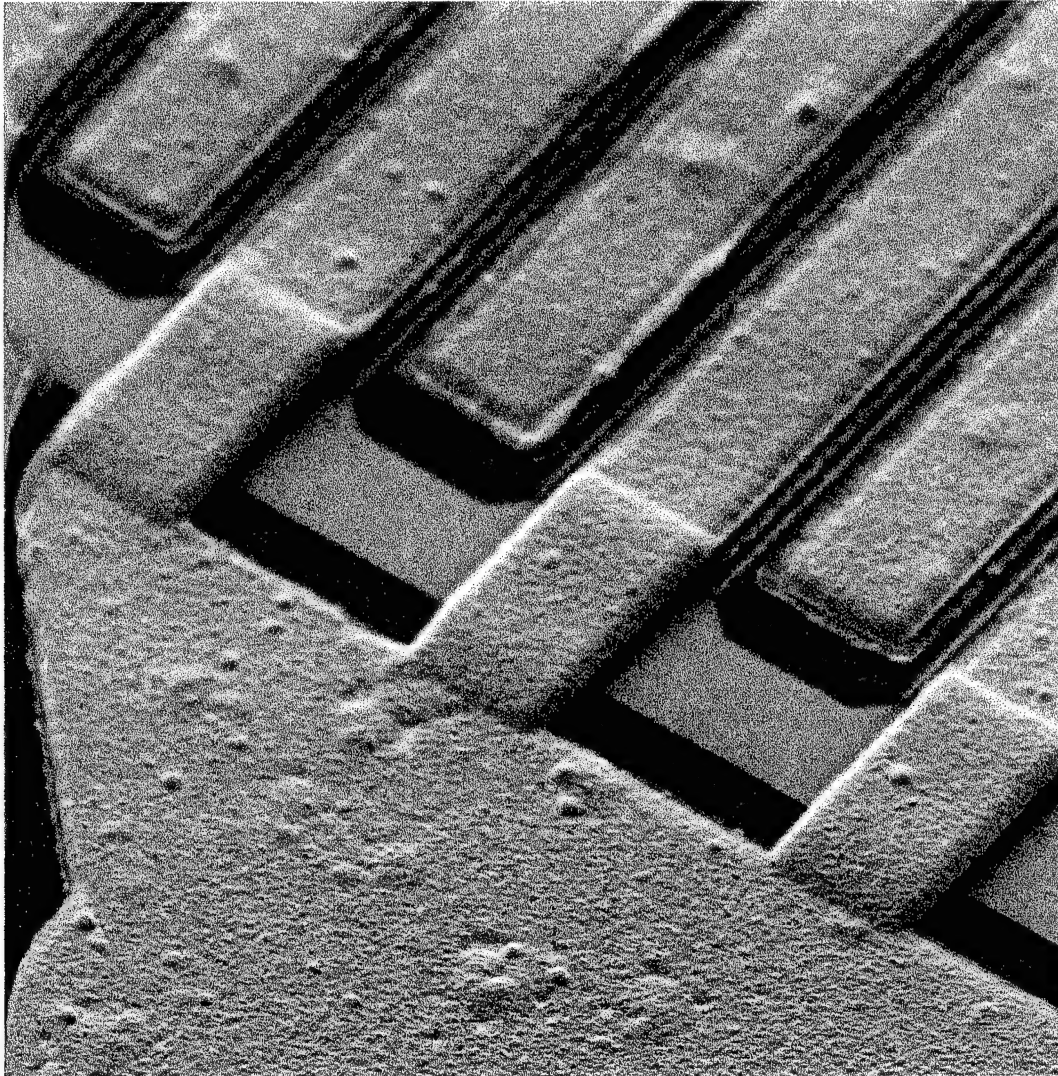


Figure 15. SEM of airbridge fabricated on AlGaN JFET.

### 2.3.1 High Temperature Ohmic Contacts

A critical device parameter influencing the performance of FETs for power switching is the source and drain ohmic contact resistance. High resistances at the S/D contacts produces electrical losses via heat generation and can ultimately limit the device switching speed as well as the efficiency. Furthermore, the metal-semiconductor contact is often the source of device failure under operation at high temperatures. The contact reliability under temperatures of 400-500°C then becomes a significant concern for application of the devices in harsh or high power environments. For these reasons, a significant effort was undertaken to discover a low resistivity, high temperature contact system for the JFET structures.

Contact metals were patterned by e-beam evaporation and liftoff on n-GaN samples in a sequence of 200 Å Ti, 500 or 1000 Å refractory metal, and 3000 Å Au. For a baseline comparison, 2000 Å Ti/4000 Å Al contacts were annealed at 630°C for 30 s and characterized. Electrical measurements were performed with transmission line measurement (TLM) structures patterned by liftoff. Following a mesa isolation by reactive ion etching (RIE) in SiCl<sub>4</sub> plasma, the refractory samples were annealed for 30 s in N<sub>2</sub> ambient at a temperature of 875°C. Then, the refractory metallization system which yielded the best resistivity following 875°C RTA was characterized for RTA temperatures to 1000°C. Individual 1 cm<sup>2</sup> samples with identical metallization sequences were annealed at 900, 950 and 1000°C; TLM data was then collected for each sample.

Contact metallization schemes were studied before and after annealing by Auger electron spectroscopy (AES) depth profiling to examine the elemental diffusion. Depth profiling through the contact layers was accomplished with argon ion sputtering. The measurements were carried out with a Physical Electronics PHI 560 spectrometer and a differentially pumped argon ion gun. Auger spectra were acquired with a 5 keV primary beam energy, and no artifacts due to background pressure or the electron beam were detected. Sputtering was performed with a 3.5 keV ion beam focused to a spot size of approximately 0.25 mm. The beam was rastered over an area of 1.5 mm by 1.0 mm, and Auger spectra were acquired with a focused electron beam area of approximately 10 micrometers in the center of the sputter crater to avoid edge effects.

Contact resistivities are plotted in Figure 16 for the measured TLM data as a function of metal sequence. The Ti/x/Au sequences with intermediate refractory metals are identified for thicknesses of 500 and 1000 Å. Also included in the data is that for the Ti/Al contacts annealed 30°C below the melting point of Al. The 2000 Å Ti/4000 Å Al metallization and anneal at 630°C produced ohmic contacts with a high resistivity of 10.3 W·mm. The AES profile for the Ti/Al contacts revealed significant diffusion of Ti throughout the Al; furthermore, Al is present at the n-GaN surface. Since TiN formation at the Ti/n-GaN is responsible for low contact resistances, interference by any other metals which may electromigrate into the semiconductor is not desired.

Electrical testing and AES profiling of the contacts with 200 Å Ti, intermediate refractory metals, and Au revealed more details on the contact behavior during annealing. Even though a contact resistivity of 1.61 W·mm was achieved with the 875°C anneal, the use of 500 Å Pt as a blocking intermetallic layer failed to be successful. The diffusion of Au, as well as Pt, to the n-GaN persisted. Similar contacts using 1000 Å Pt limited the Au diffusion; however, Ti appeared in small concentrations throughout the Pt barrier following the anneal process. The Ti/1000 Å Pt/Au sequence yielded a minimum resistivity of 3.44 W·mm.



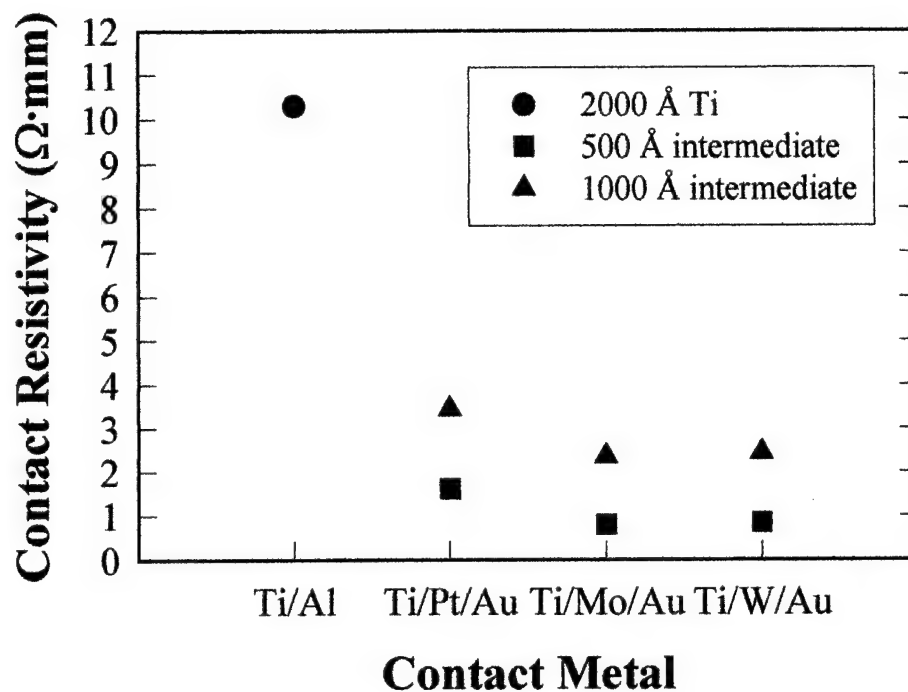


Figure 16. Contact resistivity plot for GaN ohmic contacts.

Better success with isolation of the respective metals was achieved using Mo and W intermediate layers to block both Au and Ti diffusion. As is shown in the plots of Figures 17 and 18, for Mo and W, respectively, only 500 Å of the refractory metals were required to limit Au and restrict Ti at the semiconductor interface. Among the two, the Mo intermetallic yielded somewhat steeper profiles and a minimum contact resistivity of 0.79 W·mm, verses 0.84 W·mm for 500 Å of W. Similar AES profiles were obtained with 1000 Å intermediate layers of Mo and W; however, the higher metal resistivities with respect to gold resulted in slight increases of the contact resistivities to 2.35 and 2.43 W·mm for Mo and W, respectively.

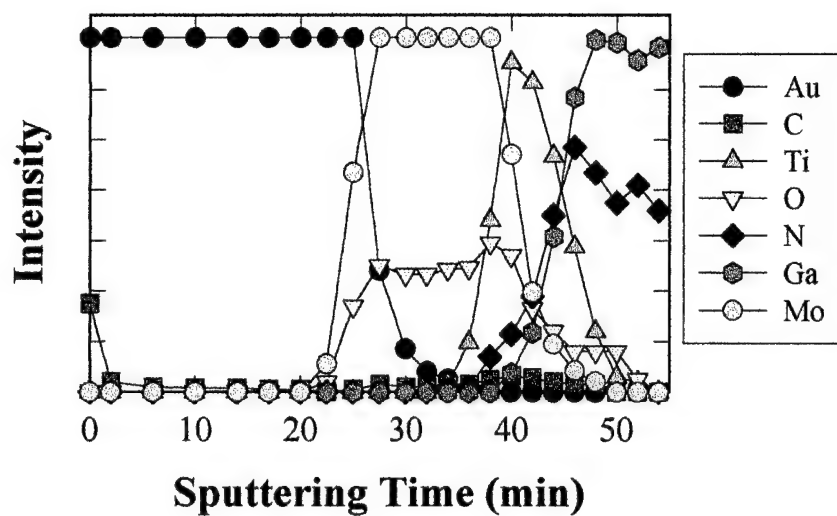


Figure 17. (a). Sputter Auger scan of Au/Ti/Mo ohmic contact before 875 ° C anneal.

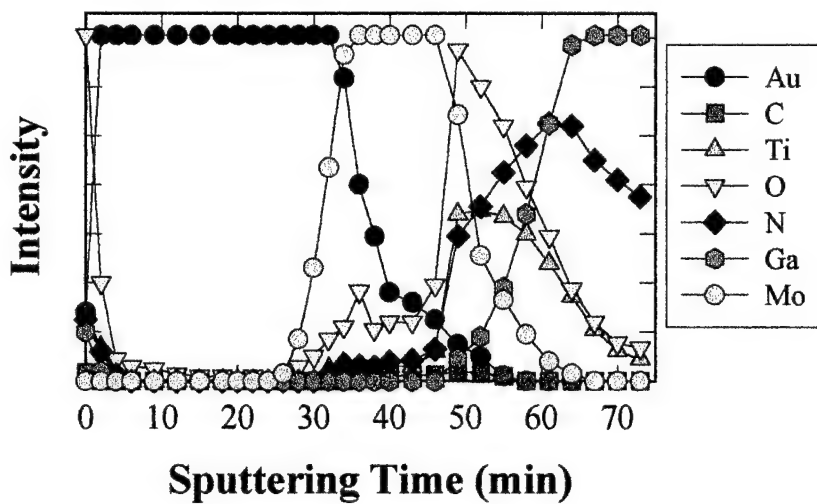


Figure 17. (b). Sputter Auger scan of Au/Ti/Mo ohmic contact after 875 ° C anneal.

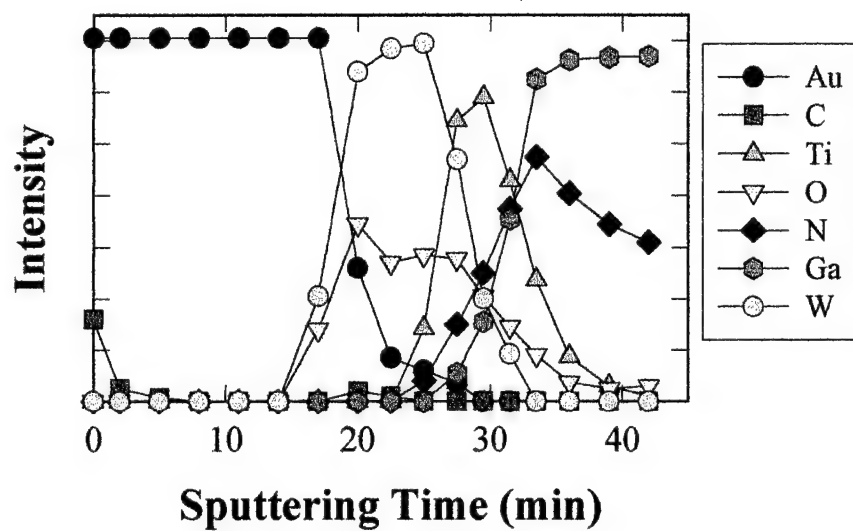


Figure 18. (a). Sputter Auger scan of Au/Ti/W ohmic contact before 875 ° C anneal.

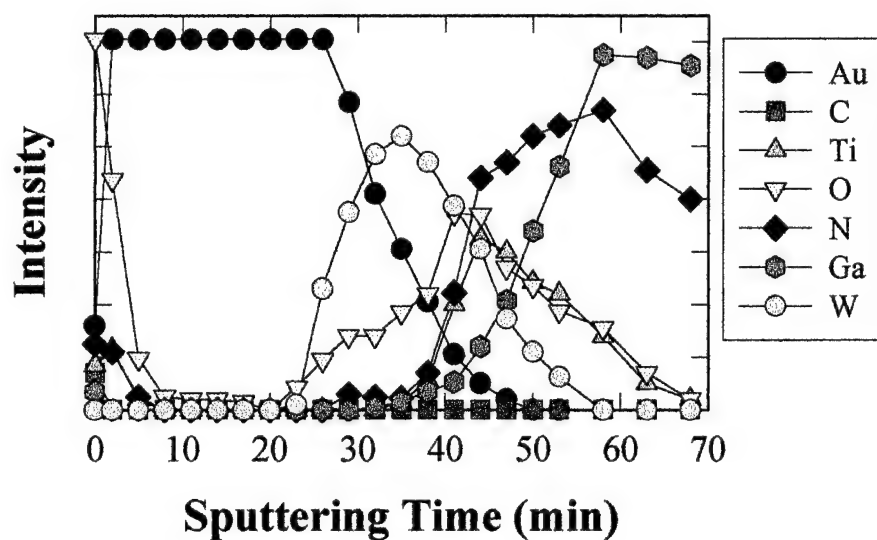


Figure 18. (b). Sputter Auger scan of Au/Ti/W ohmic contact after 875 ° C anneal.

## 2.4 JFET Test and Measurement

At present, JFET structures have been fabricated and tested with limited success. Fortunately, the cause of device failures has been identified and steps are being taken to achieve a working JFET to be detailed in a Phase II proposal. The parallel plate RIE recess step (see Figure 14 step 3) with a gate metal mask has proven to be too harsh for the Ni/Au gate contact. During the fabrication sequence, gates are deposited with smooth morphology as seen in Figure 19. However, the process step for back etching of p-GaN to expose the n-AlGaIn, resulted in significant reaction of the Au in the  $\text{SiCl}_4$  plasma by forming volatile gold chlorides. The gold chlorides might have also been re-deposited on the surface of the JFET creating short circuits.

The reactivity of the gold surface in the RIE plasma is best seen from a micrograph of the gate diode test structures shown in Figure 20. The two gate metallization fingers of the test diode exhibit a very rough surface morphology, resulting from the plasma exposure, in comparison to the as-deposited Ti/Mo/Au S/D fingers. Further investigation of the gates on JFETs revealed a more damaging effect taking place on the 1 mm structures. While the gate metals did serve as a recess mask and back etching was performed, the sharp edges of the 1 mm structures became distorted in the highly reactive plasma gas. As seen in Figure 21, jagged edges are produced at the gate which not only prevent control of the critical dimension but also can yield short circuits and high electric field points in the transistor structure. An additional scanning electron micrograph at a  $45^\circ$  angle is presented in Figure 22 which shows the etch sidewall and the attacked NiAu gate metal on a JFET structure.

To correct the problem of recessing the p-GaN epitaxial layer, two technical processes are to be investigated. First, a refractory metal gate of tungsten (W) or molybdenum (Mo) is being employed in the JFET fabrication process which should significantly reduced the reactivity in the  $\text{SiCl}_4$  plasma. Second, inductively coupled plasma (ICP) etching which employs low energy ions is being investigated as an alternative to the very high ion energy RIE process now employed. The ICP investigation is under way with the assistance of PlasmaTherm, St. Petersburg, Florida, for other p-i-n device structures, but can be transferred to the JFET process should it be successful. Unfortunately, the ICP investigation will not be completed until mid-February due to equipment scheduling delays at PlasmaTherm. The investigation of a new mask metal is underway.

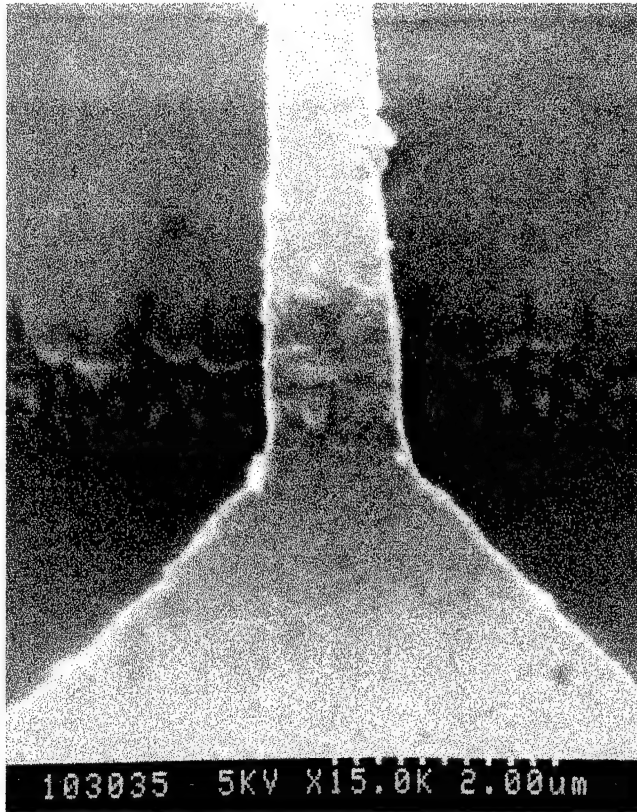


Figure 19. As deposited gate on AlGaIn JFET indicating smooth morphology.

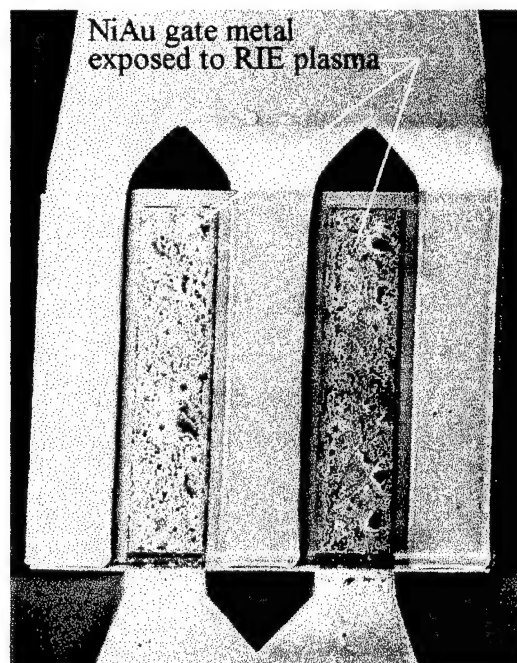


Figure 20. Test diode showing attack of the NiAu gate metal caused by the RIE process used to recess P GaN layer.

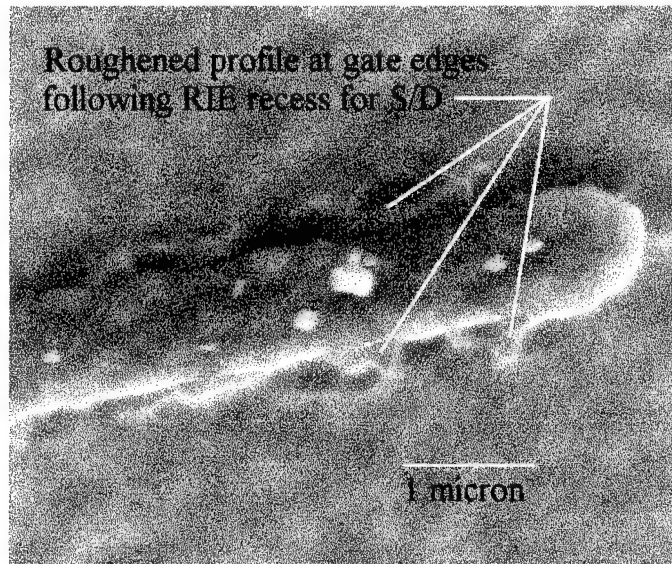


Figure 21. SEM of roughened profile of gate after RIE for source drain. This can yield short circuits and high electric field points in the transistor structure.

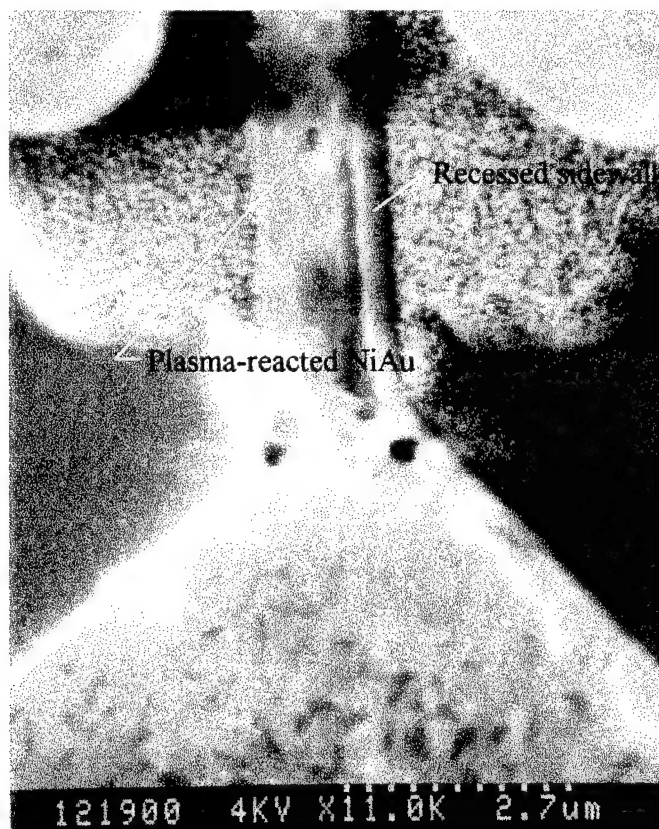


Figure 22. SEM at a 45° angle which shows the etch sidewall and the attacked NiAu gate metal on a JFET structure.

### 3.0 Conclusions and Recommendations

This final report describes SVT Associates efforts to develop AlGa<sub>N</sub> JFETs for high temperature power switching for PMDA applications. During the Phase I (6 month) effort, excellent progress was achieved using AlGa<sub>N</sub> deposited by Molecular Beam epitaxy onto sapphire substrates. Although operational JFETs were not achieved during the Phase I effort, the cause of the device failures have been identified. Working JFETs are expected by the Phase II proposal submission. The following conclusions can be reached about the Phase I program.

1. MBE is capable of producing enhanced 2-deg HEMT structures. This was demonstrated by Hall measurements as a function of temperature. MOCVD grown samples have reached much high mobility for similar structures. Work will be needed during the Phase II effort to improve this number through optimizing the buffer layer and improving AlGa<sub>N</sub> growth conditions.
2. Processing of AlGa<sub>N</sub> FET still needs to be optimized during Phase II. The main step which needs to be improved is the reactive ion etch process for both MESA and P gate recess. The current process destroys the gate metal which lead to gate leakage. A selective RIE process should be developed to stop at the AlGa<sub>N</sub> layer and remove just the P Ga<sub>N</sub>. Non-uniform etching will destroy yield and any RIE induced damage will degrade or destroy device performance.
3. High temperature testing of the JFET was not demonstrated since processing problems prevented device operation. We had hoped to determine this during the Phase I program. The Phase II program will need to address this question in the first 6 months.

We feel the Phase I program was extremely successful. Enhanced mobility was observed in AlGa<sub>N</sub> HEMT structures. A JFET mask set was designed and used to develop the processing steps needed for JFET fabrication. Several two inch wafers of AlGa<sub>N</sub> JFET structures were fabricated and tested. Based on the success of the six month program, we are now in discussion with two investment groups for the matching Phase II funding required by BMDO. We strongly recommend continued funding of this program.

## 4.0 Appendix

This is a copy of a paper presented at the 1996 International MBE conference, Malibu CA.

### Optimization of AlGa<sub>N</sub> films grown by RF Atomic Nitrogen

#### Plasma using In-situ Cathodoluminescence

J.M. Van Hove\*, P.P. Chow, A.M. Wowchak, J.J. Klaassen, M.F. Rosamond and D. R. Croswell

SVT Associates, 7620 Executive Drive, Eden Prairie MN 55344

\*(612) 934-2100 ext. 225, Fax number (612) 934-2737, jvanhove@svta.com

#### Abstract

*In-situ* cathodoluminescence (CL) is presented as a technique for determining film composition, optical quality, doping levels, and temperature of MBE grown group III nitride films. Excitation of the films is done with either the Auger or RHEED electron gun operating between 1 to 10 KeV. The CL emission is monitored using a 3 nm resolution monochromator. Optimization of the GaN growth process using a RF atomic nitrogen plasma source is discussed using *in-situ* cathodoluminescence to reduce the "yellow" defect level present in GaN. Composition and quality of Al<sub>x</sub>Ga<sub>1-x</sub>N films are shown to be quickly determined from the peak position and width. This is extremely useful in the nitride system where reflection high energy electron diffraction (RHEED) oscillations are not routinely observed. Measurement of the substrate temperature during GaN growth is demonstrated by monitoring the shift in band edge position with temperature. P type doping and MQW levels observed by CL are shown to allow quick optimization of device and material properties.



## Introduction

Interest in the group III (Al, Ga, In) nitrides and their ternary and quaternary alloys has increased dramatically with the recent progress in developing blue semiconductor lasers. Other devices such as high temperature, high power electronics and solar blind UV detectors are being developed in this wide band gap material system. While much of the growth of group III nitrides has been done with metal-organic chemical vapor deposition (MOCVD), recent progress has been made in molecular beam epitaxy (MBE) of these materials. The advancement of MBE in nitride growth is due in part to the improvement of nitrogen sources. The demonstration of 1  $\mu\text{m/hr}$  growth rates using both RF atomic nitrogen plasma sources and  $\text{NH}_3$  injectors has allowed MBE grown material to achieve comparable quality to MOCVD material [1].

One advantage MBE has over other growth techniques is the ability to monitor the growth process *in-situ*. Reflection high energy electron diffraction (RHEED) is now a commonly used *in-situ* technique for calibration of composition and growth rates for most III-V materials. Unfortunately, RHEED oscillations have only been observed under limited conditions for nitride growth. This makes film composition difficult to determine quickly *in-situ*. In this work, we present the use of *in-situ* cathodoluminescence (CL) for determining film composition, optical quality, doping levels and temperature of AlGaIn films.

Cathodoluminescence is an optical technique which uses an electron beam to excite the film. The resulting emission provides material information similar to that obtained by photoluminescence, such as the position of the band edge and the mid gap energy levels [2]. This technique has been used by Rouleau and Park to monitor *in-situ* the blue/green CL emission from MBE grown ZnSe films [3]. A significant advantage of *in-situ* CL is that it can be accomplished using a standard RHEED gun present in most MBE systems. Dispersion of the RHEED streak fluorescence through a simple monochromator /detector allows the band gap of the deposited material to be determined. From this measurement, the composition of  $\text{Al}_x\text{Ga}_{1-x}\text{N}$  and  $\text{In}_x\text{Ga}_{1-x}\text{N}$  films can be determined. The substrate temperature, a critical yet often poorly determined parameter, can be measured from the band gap shift with temperature. This is especially useful for group III nitrides grown on transparent sapphire as interference from the substrate heater hinders pyrometer measurements. The optical quality of the deposited film can also be evaluated from the FWHM of the band-edge emission, and qualitative assessment of the doping level can be made from the structure of the CL emission.

## Experimental

Figure 1 shows a schematic of the *in-situ* cathodoluminescence setup used in the MBE growth chamber [4]. A collimator lens mounted on a retractable bellows stage is brought in close proximity to the epi-wafer surface for quick *in-situ* analysis and can be withdrawn behind the cryo panels for protection during material deposition. CL excitation is done with the RHEED electron gun at 10 KeV while still observing the RHEED pattern. The emitted light was measured with a 1/8 meter (3 nm resolution) monochromator and PMT detector. A similar CL setup equipped with a fixed lens system is used with the Auger electron gun in the MBE analysis chamber

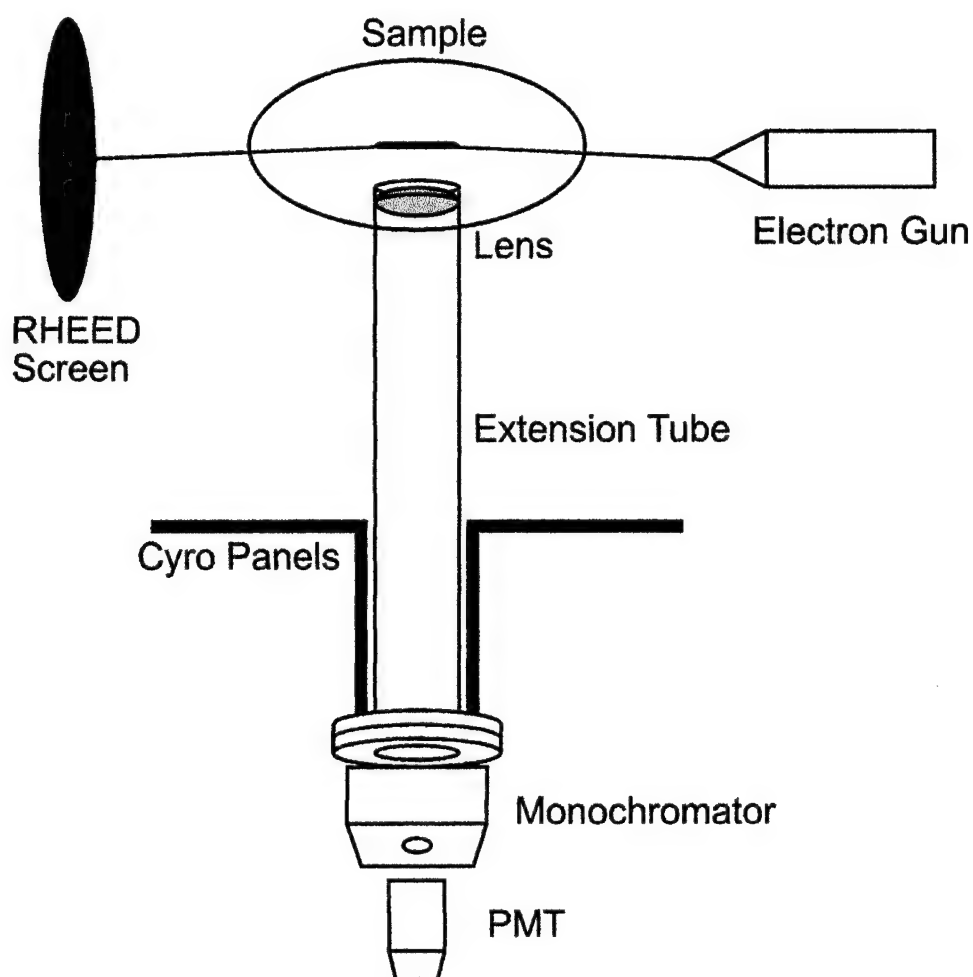


Figure 1. *In-situ* CL setup used in the MBE growth chamber. A moveable stage allows the lens assembly to be brought close to the RHEED streak. CL excitation is done with the RHEED electron gun at 10 KeV while observing the RHEED pattern. The emitted light is measured with a 3 nm monochromator and PMT detector. A similar fixed lens system was used in the preparation chamber with the Auger electron gun used to excite the film.

An atomic RF plasma source developed specifically for the growth of MBE nitride was used for this work and has been described previously [5]. The basic concept is to create a plasma of nitrogen with the use of a RF field. RF energy (200 to 550 W) is fed into the gun through a water cooled copper coil. A pyrolytic boron nitride (PBN) tube with a changeable nozzle is centered between the RF coils. Nitrogen is introduced to the tube with a leak valve and a plasma is created within the tube. Flow rates of 2 to 3 sccm of nitrogen is enough to produce growth rates around 1  $\mu\text{m/hr}$ . Elemental Ga and Al supplied from effusion cells were used for the group III elements. Mg doping was done using a conventional effusion cell while Si doping was done using a compact e-beam source. Sapphire (0001) was used as the substrate with a low temperature AlN buffer layer grown prior to GaN deposition. Growth temperatures ranged between 750 and 900  $^{\circ}\text{C}$  and a Ga rich III-V flux ratio was used. X-ray diffraction taken from a 1  $\mu\text{m}$  thick GaN on AlN/sapphire substrate using this technique shows a (0002) diffraction peak with a full width half-maximum of 39 arc seconds which is comparable to the best MOCVD X-ray results [6].

## Results and Discussion

Figure 2 shows the CL spectrum from a 1  $\mu\text{m}$  thick layer of GaN on sapphire. These scans were taken at a beam voltage of 4 KeV in the analysis chamber of the MBE system. The CL intensity is plotted on a log scale to highlight the yellow emission level which is present in most GaN films [7]. The log scale reveals considerable information lost in traditional linear plots. Figure 2 (A) shows the room temperature CL emission from an unintentionally doped n type  $10^{16} \text{ cm}^{-3}$  GaN film. This film shows very little yellow emission around 550 nm but has a sharp band edge peak with a FWHM of 66 meV. Figure 2 (B) shows the room temperature CL spectrum from a GaN film deposited under non-ideal conditions. The extremely large yellow emission peak centered around 550 nm is possibly due to the presence of oxygen and carbon in the GaN film. Similar yellow emission levels are observed under low growth temperatures, high N/Ga flux ratios, and on poor quality AlN buffer layers. Using the *in-situ* CL scans, both the yellow defect emission level and the FWHM of the GaN band edge can be measured quickly and growth conditions can subsequently be adjusted.

The *in-situ* CL scans are extremely useful for optimizing Mg doped P type GaN. MBE grown Mg doped films are P type as grown, but control of the doping level remains a problem for GaN film growth. This is due in part to the low sticking coefficient of Mg at the growth temperature used. Figure 3 shows a CL spectrum from a 1  $\mu\text{m}$  thick layer of Mg doped P type GaN on sapphire. The CL intensity is plotted on a log scale. The Hall carrier concentration of this film was measured to be  $10^{18} \text{ cm}^{-3}$  but the incorporated Mg is expected to be much higher. The band edge emission is still present, but is now considerably broadened by the heavy Mg level (compared with the undoped GaN CL shown in Figure 1 (A)). At higher doping levels, the band edge peak is replaced by a strong peak centered around 390 to 400 nm. This is in contrast to MOCVD grown P type GaN which shows a emission level centered around 425 to 450 nm [8]. Figure 3 also

shows a sharp emission peak at 694 nm due to UV excitation of the  $\text{Cr}^{+3}$  impurity in the sapphire.

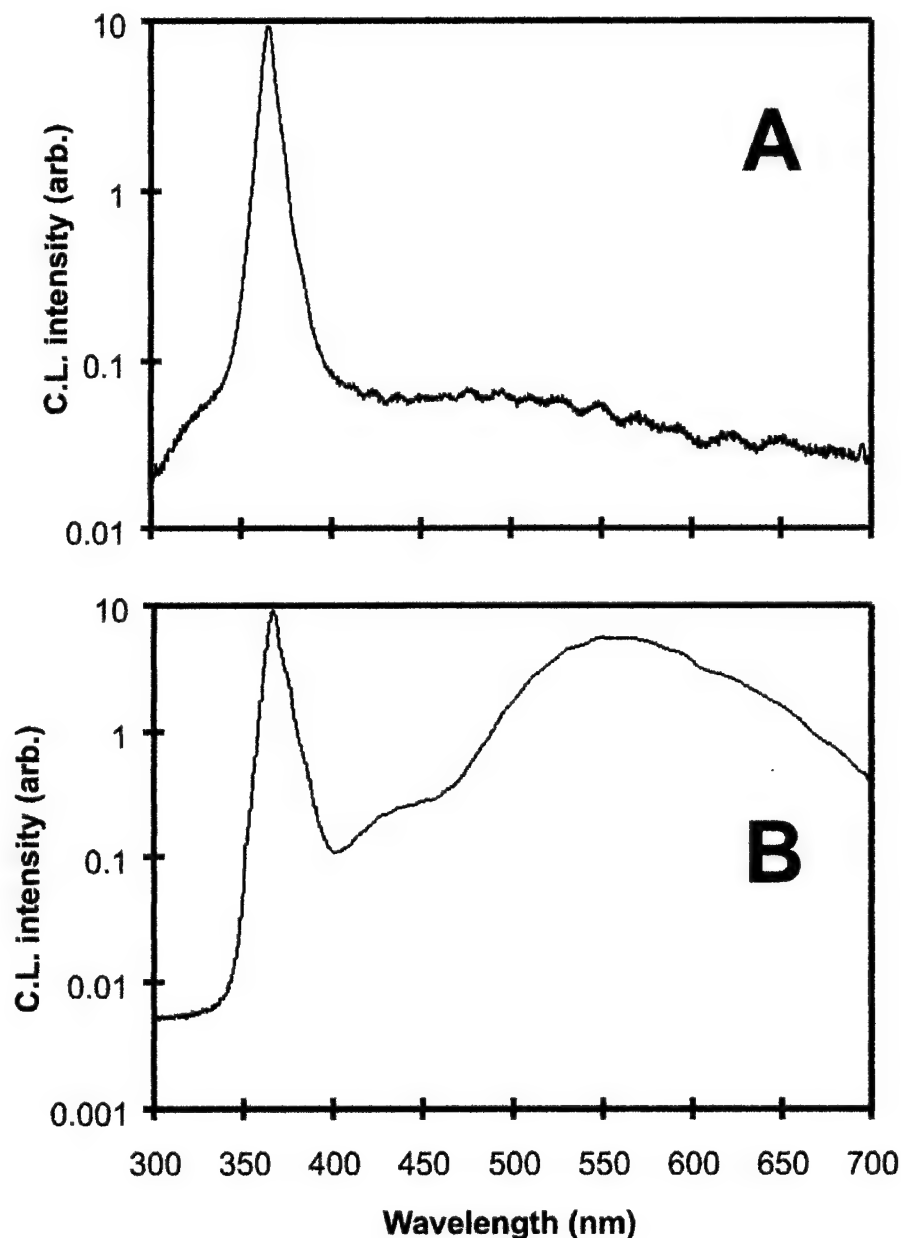


Figure 2. *In-situ* CL spectrum from 1  $\mu\text{m}$  of GaN on sapphire taken after growth at two different growth conditions. The CL intensity is plotted on a log scale to highlight the yellow emission level. (A). Room temperature CL emission from n type  $10^{16} \text{ cm}^{-3}$  GaN showing very little yellow emission at 550 nm. The FWHM of the band edge peak is 66 meV. (B) Room temperature CL from GaN deposited in an unoptimized MBE system. Extremely intense yellow emission centered around 550 nm is observed. The yellow defect emission level and the FWHM of the GaN band edge can be measured in-situ and growth conditions adjusted.

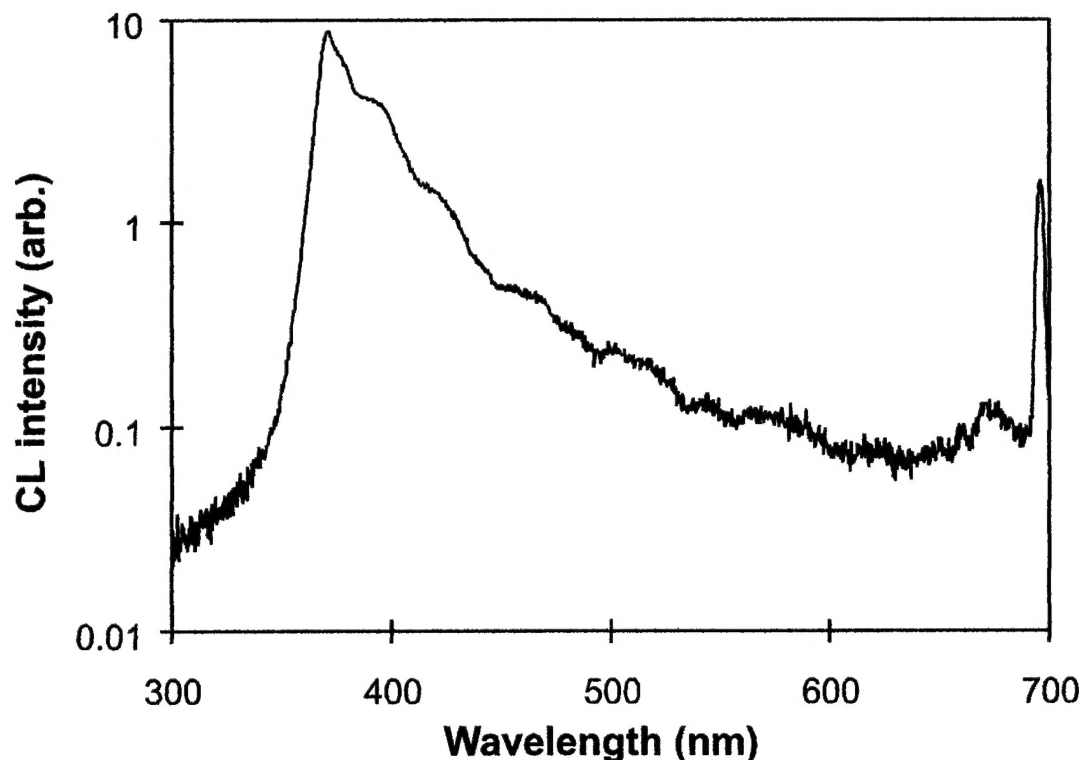


Fig. 3

Figure 3. *In-situ* CL spectrum from 1  $\mu\text{m}$  of Mg doped P type GaN on sapphire. The CL intensity is plotted on a log scale. Hall carrier concentration of this film was  $10^{18} \text{ cm}^{-3}$ . The band edge emission is broadened by the heavy Mg level when compared to the undoped GaN CL shown in Figure 1 (A). Emission from  $\text{Cr}^{+3}$  in the sapphire substrate is observed at 694 nm due to strong UV excitation of the substrate from the p-type film.

A major advantage of *in-situ* CL is that determination of the composition of AlGaIn films by measuring the band gap of the deposited material. From this measurement, the Al content can be determined [9]. Figure 4 shows the CL spectrum from a multiple quantum well sample deposited on a  $\text{Al}_{0.15}\text{Ga}_{0.85}\text{N}$  clad layer on sapphire. The CL intensity is plotted on a linear scale. The MQW region consisted of 5 repeats of 50  $\text{\AA}$   $\text{Al}_{0.10}\text{Ga}_{0.90}\text{N}$  barriers and 30  $\text{\AA}$  GaN wells. Emission from the quantum well region is clearly observed at 358 nm and from the clad layer at 320 nm. The 10% barrier level is weakly observed around 335 nm. Emission has been observed from  $\text{Al}_x\text{Ga}_{1-x}\text{N}$  for  $x = 0$  to 1. CL is extremely useful for scanning high Al content films where deep UV lasers are costly for PL measurements. The CL spectra are shown at three different electron beam voltages to demonstrate CL's ability to depth profile a structure. At higher beam voltages, the lower clad emission becomes dominant due to the increased penetration of the electron beam and the thickness of the clad layer.

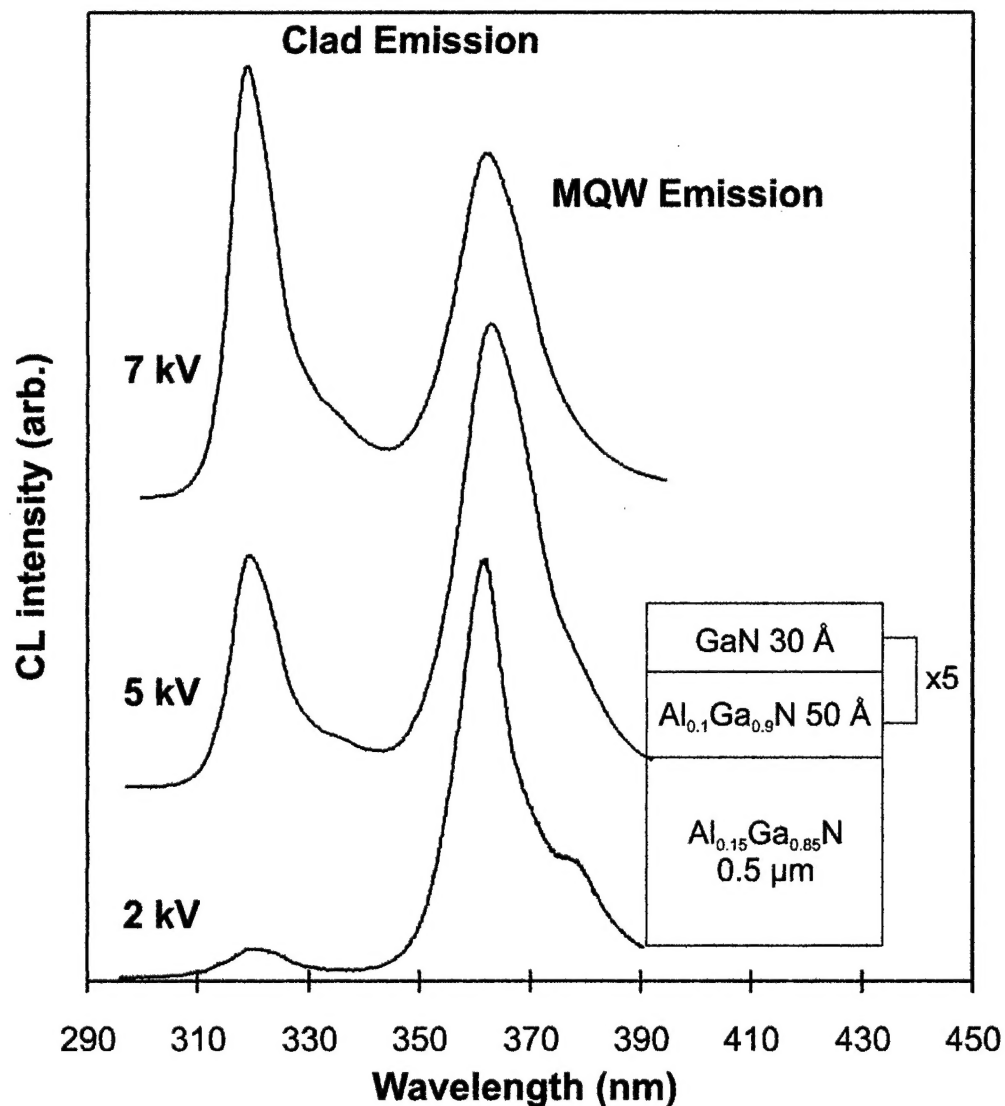


Figure 4. *In-situ* CL spectrum from a multiple quantum well sample deposited on to a  $\text{Al}_{0.15}\text{Ga}_{0.85}\text{N}$  clad layer on sapphire. The CL intensity is plotted on a linear scale. The MQW region consisted of 5 repeats 50 Å of  $\text{Al}_{0.10}\text{Ga}_{0.90}\text{N}$  barriers and 30 Å GaN wells. Emission is clearly observed from the quantum well region around 358 nm and from the clad layer at 320 nm. The 10% barrier level is weakly observed around 335 nm. The CL spectra are taken at three different electron voltages to demonstrate CL's ability to depth profile a structure. At higher beam voltages, the lower clad emission becomes dominant.

Measurement of the substrate temperature for GaN growth is particularly difficult due to the transparency of sapphire from the IR to the UV. This is compounded by the lack of any well defined change in the RHEED pattern after oxide removal for calibration of an optical pyrometer. Figure 5 shows the CL spectrum from a 1  $\mu\text{m}$  thick layer of GaN on sapphire as a function of growth temperature. These scans were taken in the growth chamber with the RHEED electron gun at 10 KeV. The CL intensity is plotted on a linear scale. The figure shows the band edge peak as the substrate temperature is increased. The temperature is determined from the known shift in the energy gap with temperature [10,11]. Considerable broadening of the peak is observed at higher temperatures, but the intensity of the CL emission dropped only a factor of three from room temperature to 500° C. Above this temperature, the UV peak position was not determined due to overlapping emission from the substrate heater filaments. Improvements minimizing this interference will allow measurement of the absolute substrate temperature during growth at 800° C.

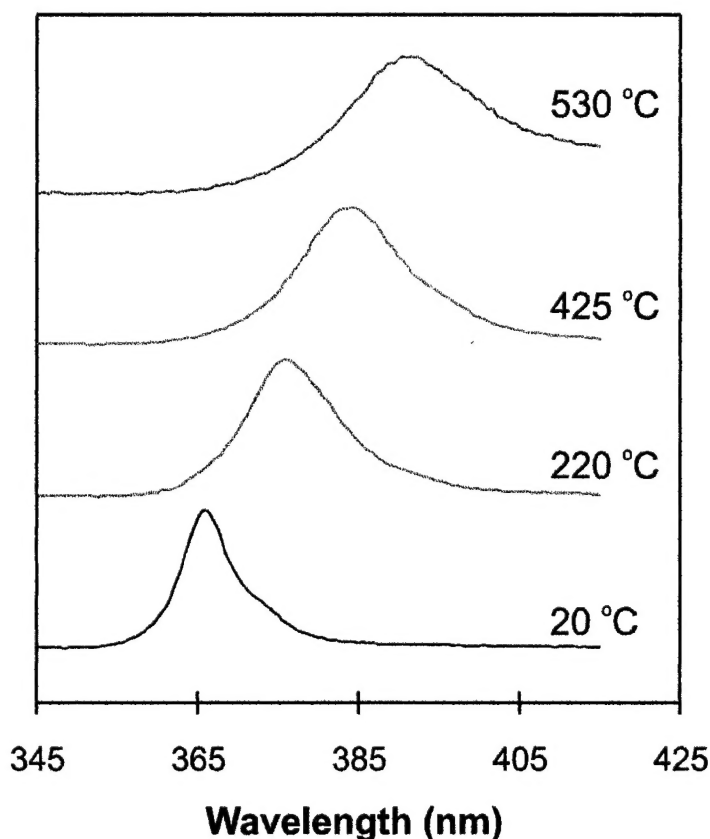


Figure 5. *In-situ* CL spectrum from 1  $\mu\text{m}$  of GaN on sapphire as a function of growth temperature. The CL intensity is plotted on a linear scale. The temperature given is based on the band edge position vs temperature from reference 9 and 10. Measurement of the temperature during growth at 800° C should be possible with an improved substrate holder to reduce light from the heater filaments.

## Summary

Reliable analysis techniques are necessary for the continued advancement of group III nitride technology. *In-situ* CL is presented as a valuable technique for determining film composition, optical quality, doping levels, and temperature of MBE grown nitride films. It is a straightforward technique which utilizes existing RHEED and/or Auger equipment for a new purpose, and can be readily retrofitted to older MBE systems.

## Acknowledgments

This work was supported in part by NASA Contract NAS5-38054 (D.A. Mott) , BMDO Contract NOOO14-96-C-0251, monitored by C. Wood ONR, and BMDO Contract DASG60-96-C-0120, monitored by M. McCurry, Army Space Command.

## References

- [1]. J.M. Van Hove, G. Carpenter, E. Nelson, A. Wowchak, P.P Chow, 1995 Chemical Beam Epitaxy Conference, accepted for publication J. Crystal Growth.
- [2]. B. G. Yacobi, D.B. Holt, J. Appl. Phys. 59, (1986) R1.
- [3]. C.M. Rouleau and R.M Park, Appl. Phys. Lett. 60, (1992) 2723.
- [4]. SVT Associates Model LMCL3, Patent disclosure filed.
- [5]. J.M. Van Hove, G.J. Cosimini, E. Nelson, A.M. Wowchak, P.P Chow, J. Crystal Growth 150 (1995) 908.
- [6]. K. Doverspike, L.B. Rowland, D.K. Gaskill, and J.A. Freitas, Jr., J. Electronics Mat. 24 (1995) 269.
- [7]. J. Neugebauer, C. G. Van de Walle, Appl. Phys. Lett. 69, (1996) 503.
- [8]. I. Akasaki, H. Amano, M. Kito, and K. Hiramatsu, J. Lumin 48/49, (1991) 666;
- [9]. S. Yoshida, S. Misawa, and S. Gonda, J. App. Phys 53, (1982) 6844.
- [10]. J. I. Pankove, J. E. Berkeyheiser, H.P. Maruska, and J. Wittke, Solid State Commun. 8, (1970) 1051.
- [11]. B. Monemar, Phys. Rev B 10, (1974) 676.